Research article

The efficiency of *Raphia hookeri* adsorbent in indigo carmine dye removal: Economy depth via chemometrics

Adejumoke A. Inyinbor [a,b,*], Deborah T. Bankole [a,b], Pamela Solomon [a], Temitope S. Ayeni [a], Adewale F. Lukman [c]

[a] *Department of Physical Sciences, Landmark University, P.M.B 1001, Omu Aran, Nigeria*
[b] *Landmark University Clean Water and Sanitation Sustainable Development Goal, Landmark University, Omu Aran, Nigeria*
[c] *Department of Mathematics, University of North Dakota, Grand Forks, ND, USA*

A B S T R A C T

The remediation of dye pollutants remains a concern in contemporary water management practices. Hence, the need for efficient and cost-effective techniques for dye removal from wastewater. In this study, the epicarp of *Raphia hookeri* fruits was treated with orthophosphoric acid for enhanced porosity and efficiency in the uptake of Indigo carmine dye (ICD). Treated *Raphia hookeri* fruit waste (RHPW) presented morphologically distributed pores as well as high porosity with Branneur-Emmet-Teller (BET) surface area of 945.43 m^2/g. RHPW displayed functional groups suitable for adsorption. The maximum ICD uptake was observed at pH 5 while the maximum uptake (q_{max}) was 20.41 mg/g in the concentration range of 2–10 mg/L. Freundlich isotherm and Pseudo-second order kinetics well-described equilibrium and kinetics data respectively. This indicated a multilayered adsorption. The Dubinin-Radushkecich model energy value was 40.82 kJ/mol, indicating chemical adsorption. The ridge regression, the Lasso and the Elastic net statistical models were used to establish a positive relationship between the various adsorption operational parameters studied. Lasso provided the best result based on the estimated mean squared error. The RHPW-ICD adsorption system was more favorable at room temperature, as the removal efficiency decreased with temperature rise. The findings established *Raphia hookeri* fruit epicarp as an economical and sustainable precursor for the preparation of potent adsorbent for Indigo carmine dye removal. This can find possible application in wastewater treatment.

1. Introduction

The accumulation of dyes in the environment can be attributed to the effect of increased industrialization and improper waste management. Industrialization and urbanization are part of human advancement and accomplishments. Many manufacturing industries are known consumer of huge volume of water and produces a substantial quantity of wastewater. Hence, there has been a rising concern about pollution problems in industrialized developing countries [1,2]. These wastewaters sometimes contain organic pollutants that have been linked with various negative environmental and human health concerns [3]. These pollutants can persist, accumulate, and magnify in the environment. Hence, upsetting the aquatic life directly and indirectly via the food chain [1]. Dyes are large organic molecules and are known to persist in the environment. A low concentration of dyes in the effluent can nonetheless

---

produce massive harmful compounds through various chemical reactions such as oxidation and hydrolysis [4]. Chronic exposure to some dyes and their breakdown products has been linked to health issues such as skin irritation, allergies, and carcinogenic potential. However, the health concerns vary depending on the type of dye and the level of exposure.

Dye contamination can disrupt aquatic food chains by hurting or killing primary producers, which in turn influence higher trophic levels. Some dyes can bioaccumulate in aquatic organisms, resulting in larger concentrations among predator species [5]. Indigo Carmine (ICD) belong to a class of water-soluble semi-synthetic dye. ICD has been used for various industrial applications including the food (such as desserts, beverages and candies), textile, cosmetics, pharmaceuticals and plastic industries [4,5]. ICD is a threat to aquatic life, and the byproducts of its degradation are known to be mutagenic, carcinogenic, allergenic, and highly toxic, resulting in a variety of health issues [8]. Another environmental concern is that ICD can interact with metal ions which can alter their physiochemical properties, stability and toxicity level [9].
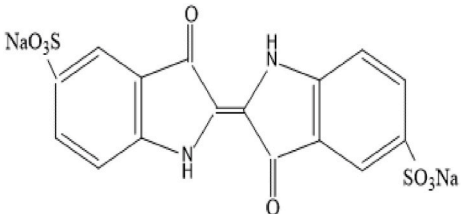
Various techniques has been previously employed in ICD removal viz reverse osmosis [10], electrochemical destruction [11], ozonation [12], irradiation [13], membrane filtration [14] and adsorption [1]. Of all these techniques, adsorption seems to be one of the most intriguing techniques. Adsorption is an inexpensive, simple, adaptable, and highly efficient method for removing low-concentration pollutants. However, adsorption is limited due to the expensive nature of commercial activated carbon. Hence, a great search for alternative to activated carbon. Cost is an important factor to consider when making a choice of adsorbent precursor, specifically in developing countries. Over the past years, the use of agricultural wastes such as palm kernel shell [1], *Bilghia sapida* seed pods [15], coconut husks [16], orange peels [17], *Raphia hookeri* pericarp [15,16], etc, as adsorbent precursors for adsorbent preparation have helped to significantly reduce cost, when compared to commercial activated carbon. Although the efficiency of these wastes, in their raw/unmodified state may not be optimal. However, the instantaneous availability and the synergistic effect of different modification methods makes agrowastes an attractive choice [17–19].

Adsorbent is a carbon-rich substance produced by pyrolysis of organic wastes, including biomass, manure, and sludge [22]. Adsorbents have multiple applications, including carbon sequestration and storage [23], soil amendment aid [24], supercapacitors [23], energy catalysis [25], and adsorption [25]. The preparation of adsorbent from diverse wastes has been examined for adsorption of several pollutants such as heavy metals and organic pollutants [22,23]. It has gained relevant attention in adsorption processes because of properties like pollutants retaining ability, porous structure, stability and high surface area [24–28]. Interestingly, we can achieve environmental sustainability by using wastes to eliminate toxic wastes. Several studies have demonstrated the effectiveness of adsorbent in removing various pollutants, such as dyes [29,30], heavy metals [31,32], and organic compounds [33,34], from wastewater.

Raphia hookeri is an agrowaste belonging to the Palmecea family [15,17–20], that grows wide in the southern of Nigeria. The plant is widely recognized in Gambia, Cameroon, Congo, Angola, Nigeria and Gabon. Raphia palm grows naturally and abundantly in the south-southern states of Nigeria, and hence a suitable adsorbant precursor considering its wide availability and low-cost [38]. Although *Raphia hookeri* wastes (RHPW) has been utilized in the uptake of a few pollutant which include dyes such as Methylene blue [39], Erythrosine B [38], acetaminophen [19], Rhodamine B [29], and heavy metals such as Copper [28], Cadmium [40], Lead [41]. To our extent of awareness, no previous report exists for the use of RHPW in the uptake of ICD (a dye with great applications).

The objectives of this study were to utilize an economical, green and sustainable *Raphia hookeri* epicarp material in adsorbent preparation via acid impregnation cum thermal treatment. This specific treatment was intended to generate porous material suitable for the uptake of large molecule such as ICD. Also, the effects of treatments were validated using surface area, morphology and functionality characterization. The effectiveness of the prepared adsorbent in Indigo carmine dye (ICD) removal was studied using a variety of operational variables that influences the adsorption system. Isotherm and kinetic models were applied to the experimental data to envisage the adsorption nature and rate, isotherm and kinetic models were fitted using the obtained experimental data. Different statistical tools were used to justify the process economy of RHPW at high temperatures. The relationship between RHPW and different variables were further established.

Table 1
Properties of Indigo carmine dye (ICD).

Parameters	Values
Suggested name	Indigo carmine
Color Index number	73,015
C.I name	Indigotin disulfonate sodium
Class	Food dye
λ_{max}	596
Chemical formula	$C_{16}H_8Na_2O_8S_2$
Molecular weight	466.36 g/mol
Structure	

2. Materials and methods

2.1. Materials

The selected food dye was obtained from central Drug House (CDH), New Delhi, India. The properties of Indigo carmine are as listed in Table 1. All of the reagents used in this study were of analytical grade. All the stages of the experiment were conducted employing deionized water.

2.2. Adsorbent material preparation

The Raphia hookeri fruits was locally sourced from Omu Aran locality (latitude 8° 8'00"N and longitude 5° 6'00" E) Kwara State, Nigeria. The epicarp was neatly separated from the entire fruit. To ensure proper dirt removal, deionized water was used to thoroughly clean the wastes obtained. After cleaning, the sample was dried in an oven at 105 °C for 24 h. The dried sample was cut into smaller bits, milled, and sieved to a 150–215 μm size range, the sample was washed several times till filtered water were clear. The sample was then dried at 105 °C for 24 h. It was subsequently stored in a container and labelled as RHPW for further treatment and usage. An acid-activation was chosen because it is a modification technique that enhances the specific surface area, adsorptive properties, functionalities and selectivity of an adsorbent for the uptake of different adsorbates [42]. The acid-activation and carbonization were performed in accordance with the method described by Bankole et al., 2022 [15]. The cleaned epicarp of *Raphia hookeri* fruits was exposed to 98 % orthophosphoric acid as the activating agent. A 50 g sample was thoroughly mixed with 150 mL of the activating agent. The mixture was heated for 3 h with constant stirring till a pasty material was attained. The paste was taken to the furnace and charred at 350 °C for 90 min. The produced activated carbon was then thoroughly washed to pH 6.10 and oven-dried at 105 °C for 24 h.

2.3. Characterization of RHPW

RHPW characterization was undertaken in order to gain insight into the surface chemistry, porosity, morphological appearance amongst others. The physicochemical and spectrophotometric characterization of RHPW were carried out using the methods described by Ekpete et al., 2017 [43]. The pH, moisture content, volatile components, ash content, percentage fixed carbon content, bulk density were analyzed while amount of oxygen-containing compounds were determined via Boehm titration [24–26]. For the pH_{pzc} was adjusting 0.1 M NaCl between pH 1 and 12 using HCl and NaOH for acidic and basic medium respectively. A 0.1 g each of RHPW was added to each of the pre-pH adjusted NaCl solutions. The content was agitated for 24 h and the final pH was recorded. The pH_{pzc} value was obtained from the intersection of the curve of the plot pH versus ($pH_{initial}$ - pH_{final}) versus pH. Boehm titration, 1.0 g of the prepared adsorbent sample was kept in contact with a 25 mL solution of $NaHCO_3$ (0.1 M), Na_2CO_3 (0.05 M), and NaOH (0.1 M) for acidic groups and 0.1 M HCl for basic groups. The aqueous solutions were then back-titrated with HCl (0.1 M) for the acidic group and NaOH (0.1 M) for the basic group. The amount and kind of acidic sites were determined by taking into account that NaOH neutralizes carboxylic, lactonic, and phenolic groups. $NaHCO_3$ neutralizes only carboxylic groups, whereas Na_2CO_3 neutralizes both carboxylic and lactonic groups. Carboxylic groups were then measured by direct titration with $NaHCO_3$. The difference between groups titrated with Na_2CO_3 and $NaHCO_3$ was considered to be lactones, while the difference between NaOH and Na_2CO_3 was assumed to be phenols. The basic site was established by titration with HCl. The functional groups, surface morphology and RHPW surface area was investigated using Fourier Transformed Infrared (FTIR) spectroscopy (NICOLET iS5), Scanning Electron Microscopy (SEM) (JEOL JSM-7600F) and Braneur-Emmet Teller surface area analysis respectively.

2.4. Adsorption of ICD onto RHPW

A 100 mg/L standard solution of Indigo carmine dye (ICD) was prepared by dissolving 0.1 g of ICD in 1000 ml standard flask containing deionized water. The stock was used to prepare adsorbate at various working concentrations (2.5–10 mg/L). Different operational variables such as pH, initial concentration, contact time, temperature and adsorbent dosage range were investigated to the identify the optimum conditions from effective adsorption. The batch sorption studies on indigo carmine dye removal focused on pH (2–10), with an initial ICD concentration of 10 mg/L and RHPW dosage of 0.07 g. The impact of various doses (0.15g–0.25 g) of RHPW dosage was investigated using a concentration of 30 mg/L of ICD, agitated for 4 h. The temperature was varied between 298 K and 318 K on the removal of ICD using the optimum conditions obtained from effect of pH, initial concentration and time. For the effect of pH, a solution of 0.1 M HCl or 0.1 M NaOH were used to alter the pH of the indigo carmine solution. A 0.07 g of RHPW was added to a predetermined concentration of ICD solution in a 250 ml conical flask for each adsorption experiment. In a water-bath mechanical shaker (SHA-C, China) at a fixed/controlled temperature (298 K–318 K), the mixture was agitated for 4 h. Equation (1) was used to calculate the amount of ICD taken up at a given time, t, and equation (2) was used to calculate the percentage removal.

$$q_t = \frac{(C_i - C_t) \times V}{M} \tag{1}$$

$$\text{Percentage removal} = \frac{(C_i - C_t)}{C_i} \times 100 \tag{2}$$

where C_i is the starting/initial ICD concentration, C_t is the residual concentration of indigo carmine at a given time and C_f is the final concentration of indigo carmine. V represents the ICD solution volume in liters used for the sorption experiment, while M stands for the adsorbent weight (grams).

2.5. Isotherms, kinetics and thermodynamic equations for experimental data

Four isothermal models (Langmuir, Freundlich, Temkin, and Dubinin-Radushkevich) were applied to experimental data. The adsorption kinetics data were modelled employing the Pseudo first order, Pseudo second order, and Intraparticle diffusion equations (details in Table 2). The terms in the equations are defined as follows: the adsorbent's equilibrium adsorption capacity(q_e) and adsorbate equilibrium concentration in milligrams per liter (C_e). K_L in L/mg is the Langmuir constant, and q_{max} in mg/g represents the maximum monolayer adsorption capacity. K_L is a crucial quantity in computing R_L a dimensionless factor whose value explains the adsorption process's favorability. Freundlich constants n and K_F in mg/g incorporate the elements controlling adsorption intensity and capacity respectively. T (K) is the temperature, R is measured in J/mol/K and is the gas constant. Temkin isotherm, which assumes linear rather than logarithmic, reduces the heat of adsorption while ignoring both very high and low concentrations. B is the heat of adsorption constant, with formula B=R_Tb, and A is the Temkin constants (L/g). The intercept (BlnA) and slope (B) can be utilized in calculating A and B. for the kinetic equations, q_e and q_t are the amount of adsorbate adsorbed per mass of adsorbent at equilibrium and time t in minutes, respectively, K_1 is the pseudo-first-order equation rate constant (min^{-1}), K_2 (g/mg min) is the pseudo-second-order model rate constant, K_{Id} is the intraparticle diffusion rate constant with dimension mg/g $min^{1/2}$, and C is a constant (the thickness of the boundary layer surrounding the activated RHPW. For the thermodynamic studies, Temperature (T) has a dimension in Kelvin, K_o is typically determined from the quantity adsorbed and concentration at equilibrium, and R is the gas constant. The plot of K_o versus $1/T$ can be used to estimate the values of ΔS_o and ΔH_o.

2.6. Statistical validation

The statistical analysis was conducted using an online version of R Studio, a widely used integrated development environment (IDE) for the R programming language, version 2023. Statistical analysis validated and quantified the variation of dye removal with specific adsorption operational parameter.

3. Results and discussion

3.1. Characterization of RHPW

The pH determination was used to estimate the surface charge on RHPW [35,36]. The pH of RHPW was found to be 6.10 $\pm$ 0.02, which falls within the acceptable range for activated carbon [55]. The pH_{pzc} is the pH at the charge on the surface of the adsorbent is neutral. The graph of pH_{pzc} as shown in Fig. 1 was obtained via the plot of change in pH versus the initial pH. The isoelectric/point of zero charge for RHPW was obtained to be 5.00. At this point, the surface of an activated carbon is said to possess a zero charge. This implies that, at pH below the pzc, RHPW is highly protonated due excessive hydrogen ions, with an affinity for anionic pollutants. However, beyond the point of zero charge, deprotonation occurs due to excessive hydroxide ions with an affinity for cationic pollutants [56].

The values obtained for volatile matter, ash and moisture content were 7.45 %, 10.65 % and 3.24 % respectively, which were considerably low. This is an indication that the density of the adsorbent's precursor is moderately small. Hence, the prepared adsorbent

Table 2
Isotherms, kinetics and thermodynamic equations.

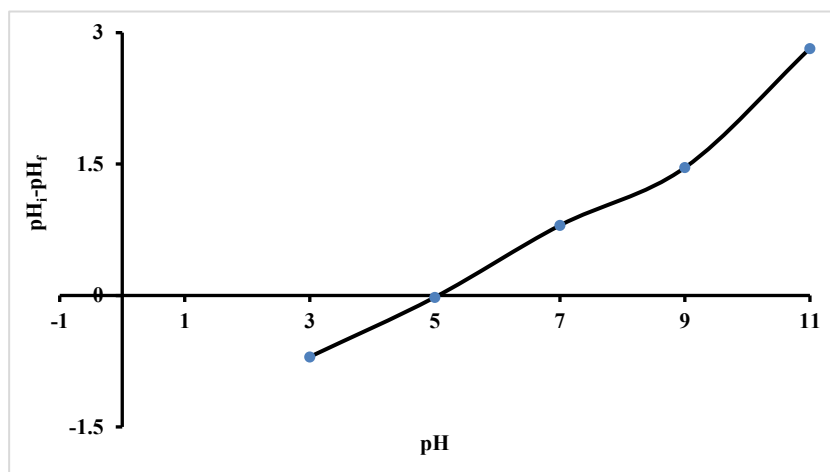| Adsorption model	Type	equation	References
kinetics	Pseudo first order	$\log(q_e - q_t) = \ln q_e - K_1 t$	[45]
	Pseudo second order	$\dfrac{t}{q_t} = \dfrac{1}{K_2 q_e^2} + \dfrac{t}{q_e}$	[46]
	Intraparticle diffusion	$q_t = K_{Diff} t^{1/2} + C$	[47]
Isotherms	Freundlich	$\log q_e = \dfrac{1}{n} \log C_e + \log K_F$	[48]
	Langmuir	$\dfrac{C_e}{q_e} = \dfrac{C_e}{q_{max}} + \dfrac{1}{q_{max} K_L}$	[49]
	Temkin	$q_e = B \ln K_T + B \ln C_e$	[50]
	Dubinin-Radushkevich	$\ln q_e = \ln q_m - A_{DRK} \varepsilon^2$	[51]
		$\varepsilon = RT \ln\left[1 + \dfrac{1}{C_e}\right]$	
		$E = -\left[\dfrac{1}{\sqrt{2 A_{D-R}}}\right]$	
Thermodynamics		$\ln K_0 = \dfrac{\Delta S^o}{R} - \dfrac{\Delta H^o}{RT}$	[52]
		$\Delta G^o = -RT \ln K_o$	

Fig. 1. pHpzc of RHPW.

(RHPW) will be a promising adsorbent for adsorption [25,39].

The Boehm titration assessment provides semi-quantitative data on RHPW surface functionalities. However, the chemical groups on RHPW could be more complex than the information provided from the Boehm titration [43]. As presented in Table 3, RHPW has a higher number of acidic functional groups (3.175) than the basic functional groups (0.682). Hence, RHPW is a cationic adsorbent as confirmed by its pH_{pzc} value (5.00).

The iodine number surface area determination is often employed to roughly evaluate the microporosity and the surface area of activated carbon. It serves as an indication for an adsorbent's porosity. RHPW has a high iodine number of 772.48 m^2/g which can be ascribed to large micropore structure and an indication of high porosity [43]. RHPW surface area (BET) was estimated to be 945.43 m2/g, confirming the adsorbents's porosity.

3.2. FTIR spectroscopy of raw and treated Raphia hookeri waste

The functional groups present on treated *Raphia hookeri* wastes (RHPW) before, after activation, and after adsorption were identified using FTIR spectroscopy. Fig. 2 shows the spectra of raw *Raphia hookeri* epicarp (RHP), acid-treated *Raphia hookeri* (RHPW) and acid-treated *Raphia hookeri* after ICD adsorption (RHPI) respectively. Observed bands at 3400 cm^{-1} on RHP represents the –OH stretching vibrations. This is because *Raphia hookeri* waste biomass contain cellulose, hemicellulose, and lignin. The –OH stretching vibration bands occurred at 3440 cm^{-1} for RHPW and at 3435 cm^{-1} after ICD adsorption. The effect of modification as well as impact of dye molecules is responsible for the observed variations. In addition, shift in bands for a particular functional group may be as a result of the active participation of such functional group in adsorption. The band located at 2920 cm^{-1} on RHP is a distinctive of –CH stretching vibrations. The disappearance of this methylene functional group on RHPW is as a result of elimination of volatile organic compounds. The C=O band shown at 1620 cm^{-1} for RHP was observed at lower wavelengths for RHPW (1610 cm^{-1}) and RHPI (1615 cm^{-1}). Chemical transformation cum active participation of a functional group in adsorption process may be responsible for such shift in absorption band [25,38].

3.3. Surface morphological characteristics of raw and treated Raphia hookeri waste

The surface morphology of RHP, Fig. 3a appears like layers of wood with scanty pores. The effect of the acid modification was visible in RHPW (Fig. 3b), in that, the original topography completely changed, creating well established and evenly distributed pores. However, after the uptake of ICD, it was clearly observed that the previously available pores have been covered up by a thick layer of the ICD molecule (Fig. 3c). The observed alteration on RHPW surface after the adsorption process confirm an effective adsorption of ICD [1,38].

Table 3
Oxygen containing functional groups on RHPW.

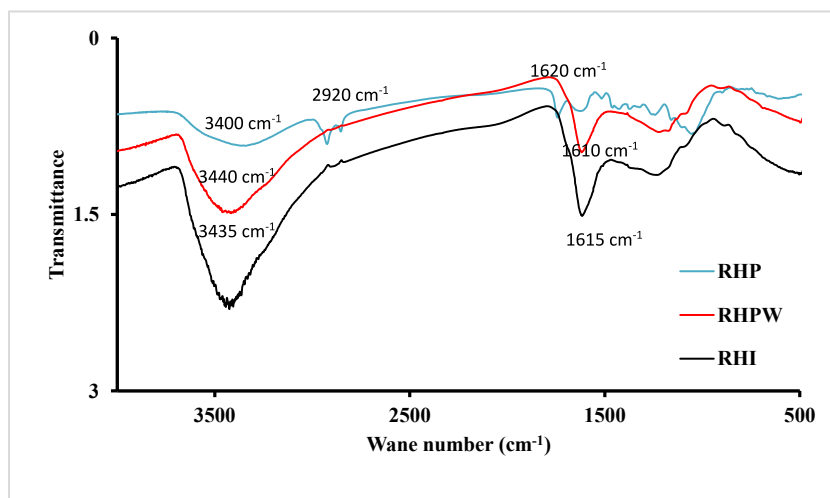| Oxygen -containing groups	RHPW
Lactones	0.905
Carboxylic	1.14
Phenols	1.13
Acidic sites	3.175
Basic sites	0.682

Fig. 2. FTIR spectra of *Raphia hookeri* before activation (RHP), after activation (RHPW) and after adsorption (RHPI).

3.4. Effect of pH on indigo carmine uptake onto RHPW

The performance efficacy of an adsorbent substantially depends on the pH of the adsorbate media [58]. This crucial factor governs the uptake of ICD onto the binding sites of RHPW. The effect of pH on ICD uptake onto RHPW was investigated by varying the pH of ICD solution between 2 and 10. As shown in Fig. 4, a high uptake was observed between pH 2 and 7 (68.47–84.95 %), with the optimum removal at the isoelectric point (pH_{pzc}) pH of 5 (84.95 %). At $pH < pH_{pzc}$, protons are available for protonation of RHPW surface, increasing the electrostatic interaction between positively charged adsorbent sites and negatively charged sites ($-SO_3$) of indigo carmine. IC is also an anionic dye with two sulphonic acid groups and two aromatic rings, which also contributed to its excellent removal efficiency at low pH. At $pH > pH_{pzc}$, the surface of RHPW is negatively charged, therefore, the electrostatic repulsion force between the adsorbates (sulphonic functional groups of pollutants) and the –OH groups on the surface of the ACs increased. The electrostatic repulsion force between indigo carmine and the adsorbent causes a decrease in adsorption capacity. Similar findings have been reported [59,60].

3.5. Effect of ICD initial concentration and contact time on the uptake of ICD onto RHPW

The interactions that occurred between the adsorbate and adsorbent as an indicator of time and ICD initial concentration (2.5–15 mg/L) at pH 5 are shown in Fig. 5. The extent of ICD uptake was very quick in the first 30 min, after which a gradual adsorption was observed as removal efficiency approached equilibrium. The rapid adsorption rate observed at the first 30 min, could be attributed to the availability of sufficient active sites on RHPW. However, at equilibrium, the adsorption rate slowed down as RHPW sites became saturated. Similar observations have been reported [1,42,43].

3.6. Isothermal studies of ICD uptake onto RHPW

The adsorption isotherms describe the possible interaction between RHPW and ICD at equilibrium. Based on underlying theories, specific model reveals specific information. The experimental datasets were fitted to Freundlich, Langmuir, Temkin and Dubinin-Radushkevich isotherm models. Langmuir adsorption model, which was first developed to characterize gas-solid phase adsorption and used to quantify and compare the adsorptive capacity of various adsorbents. The Langmuir isotherm allows for surface coverage by balancing adsorption and desorption rates.

The model assumes that all adsorption sites have equal energies. This suggests that once the adsorbate (ICD) fills up a site, there can be no interface with the adjacent sites [63]. The values of q_{max} obtained at 298 K, 308 K and 318 K were 20.41, 18.18 and 15.31 mg/g respectively as shown in Table 4. The values of the dimensionless parameter (R_L) obtained was found to be between 0.018 and 0.292. These values were generally less than one, suggesting a favorable RHPW-ICD adsorption system. The Freundlich isotherm applies to adsorption processes that occur on heterogeneous surfaces [15]. This isotherm provides an equation that characterises surface heterogeneity and the exponential distribution of active sites and their energy. The Freundlich model is applicable to a multilayer adsorption [42,45,46]. Of all the three investigated isotherms, the Freundlich model provided a best fit for the experimental data, with the R^2 values ranging between 0.987 and 0.996. which implied that multilayer adsorption occurred in the RHPW-ICD system. The Temkin model adopts that adsorption heat of the adsorbate (ICD) in the layer decreases as the surface coverage decreases as a result of ICD/RHPW interactions. A uniform binding energy distribution is exhibited, to the maximum energy [66]. The Dubinin-Radushkevich isotherm model is an empirical adsorption model that is commonly used to describe adsorption mechanisms with Gaussian energy distributions on heterogeneous surfaces. It is commonly used to distinguish between physical and chemical adsorption. The adsorption
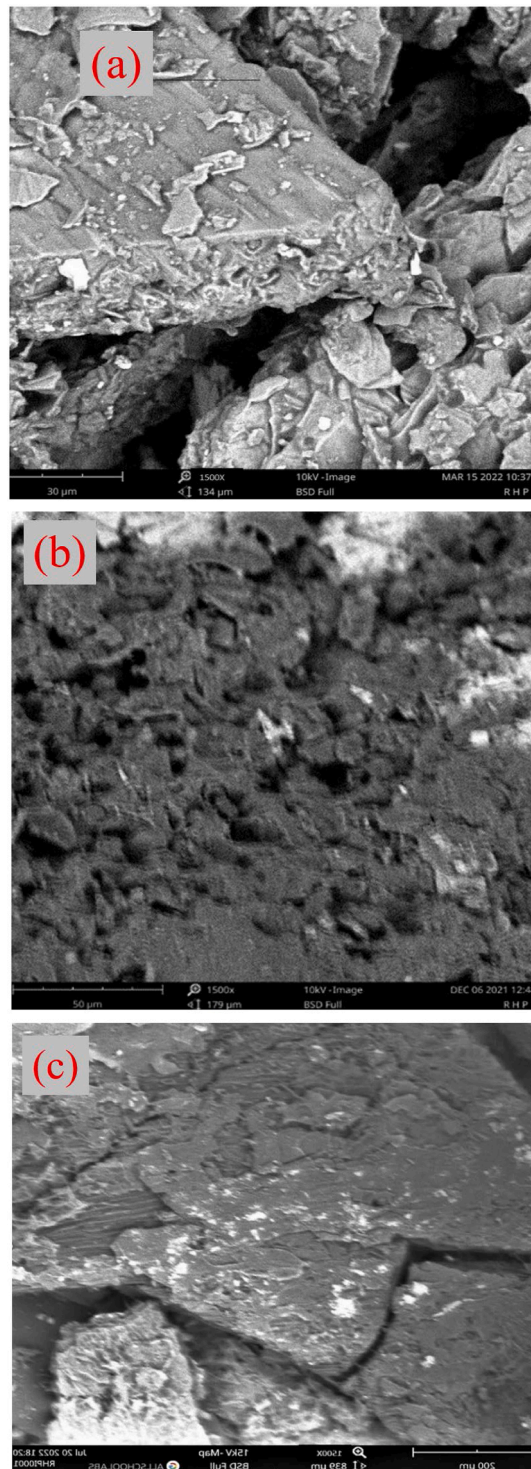
Fig. 3. Scanning electron micrograph of (a) RHP, (b) RHPW and (c) RHPI.
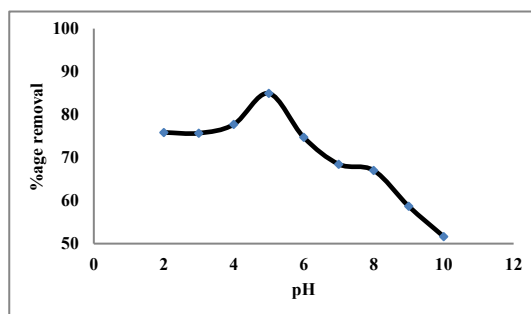
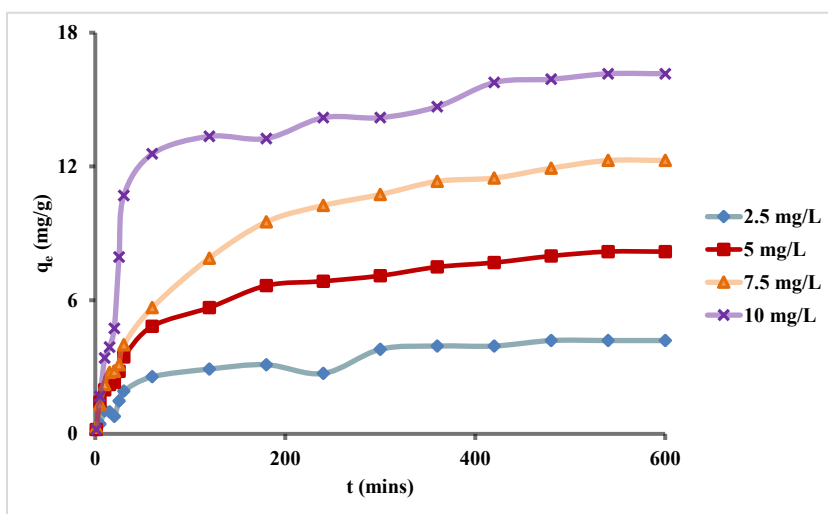**Fig. 4.** Effect of pH on indigo carmine adsorption onto RHPW.

Fig. 5. Contact time and initial concentration effect on the uptake of ICD onto RHPW.

Table 4
Isotherm parameters for the uptake of ICD onto RHPW.

Isotherms	constants	298 K	308 K	318 K
Langmuir	q_{max} (mg/g)	20.41	18.18	15.31
	R_L	0.0107–0.0614	0.0354–0.1806	0.0642–0.2918
	R^2	0.973	0.974	0.82
Freundlich	K_F (L/g)	1.1559	1.3179	1.2964
	n	1.04	1.24	1.11
	R^2	0.987	0.991	0.996
Temkin	A_T (L/g)	1.0258	1.0269	1.038
	B_T (J/mol)	627.869	473.767	426.703
	B (kJ/mol)	3.946	5.405	6.196
	R^2	0.856	0.922	0.634
D-R	q_{DR} (mg/g)	17.29	19.81	20.16
	$\beta \times 10^{-6}$ ($mmol^2\,kJ^{-2}$)	3	7	4
	E_{DR} (kJ/mol)	408.25	267.26	353.55
	R^2	0.9486	0.9814	0.9819

energy was obtained to be greater than 8 kJ/mol as shown in Table 4, indicating that the adsorption process was dominated by chemisorption. The figures representing the isotherm data plots are presented in Figures S1–S4.

3.7. Kinetics studies of ICD uptake onto RHPW

There are several possible mechanisms that could occur in RHPW-ICD adsorption system. Such mechanism could involve the migration of ICD molecules from the bulk solution to the exterior surface of RHPW, attachment of the ICD molecules to the energetic

sites on RHPW and inner diffusion of ICD within RHPW particles [67]. Either one or a combination of these mechanisms are involved in the RHPW-ICD system. The dynamics and adsorption mechanism were evaluated using the intraparticle diffusion, pseudo-second (PSO) and pseudo first (PFO) kinetic models. The values of the parameters illustrated in Table 5, were obtained from the respective linear equation of the kinetic models. The pseudo-first order model describes adsorption in a liquid-solid system. It considers that the adsorbate absorption is directly proportional to the difference between the concentration saturation level [45]. The pseudo-second order model is based on chemisorption as the adsorbate interacts with the adsorbent surface by creating a covalent chemical bond [68]. It was observed that the pseudo second order kinetics have the highest R^2 value (0.975–0.995) indicating a chemisorption. The estimated quantity adsorbed for the pseudo-second order (PSO) model was evaluated to be very close to the quantity adsorbed experimentally in comparison to the values obtained for Pseudo first order. This is a confirmation for the best fit displayed by the pseudo-second order (PSO) model. The intraparticle diffusion model is commonly used to investigate diffusion mechanisms. Adsorption on a porous adsorbent happens in multiple phases, including transport of the adsorbate from solution, film diffusion, intra-particle diffusion into pores and solid phase, and adsorption on active sites [69]. The intraparticle diffusion model shows that some other mechanism played a dynamic role in the RHPW-ICD system, as the values of intercept is greater than zero [70]. The figures representing the kinetic data plots are presented in Figures S5–S7. The initial near symmetric progressive increase in adsorption with respect to time resulted in a linear fit at the lower time range. Subsequent gradual adsorption until the time when quantity adsorbed became negligible resulted in deviation from the initial linear fit (Figures S5 and S7). This could be explained that the initial uptake of ICD onto RHPW was controlled by the intraparticle diffusion. This is validated by the correlation coefficient obtained which ranged between 0.816 and 0.946 for the concentrations studied. The subsequent gradual and negligible adsorption at higher time could ascribed to pore diffusion of ICD.

3.8. Temperature effects and thermodynamic studies on the uptake of ICD onto RHPW

A significant parameter that can help to recognize the nature of an adsorption process, is temperature. The temperature of RHPW-ICD adsorption system was varied from 298 to 318 K, and its consequence on the removal efficiency was investigated. As shown in Fig. 6, the adsorption of ICD was found to decrease from 90.61 to 79.91 % as the temperature increased from 298 to 318 K. This implies the behavior of an exothermic reaction as heat is released during the uptake of ICD onto RHPW. In addition, some bonds that exist between RHPW and ICD may be thermally unstable hence breaks at high temperature [71]. Since the highest adsorption capacity was obtained with lowest temperature, RHPW is highly economical as it does not require higher temperature or energy for effective performance. Similar findings have been reported [15,51]. The obtained values of the standard entropy change (ΔS°), Gibbs free energy (ΔG°) and enthalpy (ΔH°) as evaluated from the Van't Hoff plot, are presented in Table 6. The value of ΔS° is negative, suggesting a decreased randomness in RHPW-ICD adsorption system. The negative value of ΔH° and ΔG° indicated an exothermic and practicability of the adsorption system respectively [73].

3.9. Statistical validation

The correlation matrix in Table 7 demonstrates that there is positive relationship between the variables under study. For instance, the strong positive and significant affiliation exist between concentration and quantity adsorbed. The condition index (CI) for equilibrium time exceeds 30, which indicates potential issues with multicollinearity among the predictor variables [53,54]. Multicollinearity increases the standard errors of regression coefficients, leading to wider confidence intervals and less precise estimates of the regression coefficients. Multicollinearity caused model instability and potentially diminished the predictive accuracy of the regression model. Kolmogorov-Smirnov test and Shapiro-Wilk test (Table 8) shows that the model residual follows a normal distribution. The F-test expresses that the overall model fits well the data. Multicollinearity is a peril regarding the performance of the ordinary least squares. Due to the presence of multicollinearity in the model, we estimated the model using some other preferred methods such as the ridge regression, the Lasso and the Elastic net. The use of Lasso and Elastic Net models aligns with modern best practices in regression modelling, especially in scenarios where multicollinearity is a known issue. By incorporating these advanced

Table 5
Kinetics parameters of ICD adsorption unto RHPW.

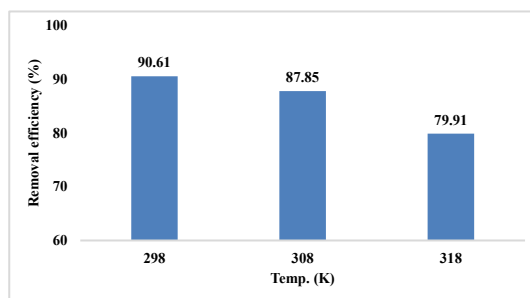| Kinetic constants	2.5 mg/L	5 mg/L	7.5 mg/L	10 mg/L
PFO				
$Q_{e,exp}$ (mg/g)	4.19	8.2	12.7	16.2
$Q_{e,cal}$ (mg/g)	3.41	6.93	11.05	14.72
K_1 (min^{-1})	0.008	0.009	0.008	0.009
R^2	0.974	0.929	0.971	0.951
PSO				
Q_e, cal (mg/g)	4.5454	7.9365	13.3333	17.8571
K_2 (g/mg/min)	79.909	30.7142	26.64	15.3035
R^2	0.991	0.975	0.987	0.991
IPD				
K_{id}	0.118	0.376	0.696	0.848
C	0.666	0.740	1.125	1.556
R^2	0.816	0.939	0.938	0.946

Fig. 6. Temperature effects on ICD uptake onto RHPW.

Table 6
Derived thermodynamic parameters for indigo carmine uptake onto RHPW.

	Pollutant	$\Delta H°$(KJ/mol)	$\Delta S°$(J/mol/K)	$\Delta G°$(KJ/mol)
				298 K 308 K 318 K
Temperature				
RHPW	ICD	−36.66	−101.89	−6.52 -4.60 -4.59

Table 7
Output for the Correlation analysis.

	CONC	EQUI	QUAD
CON	1	0.639	0.999**
EQUI	0.639	1	0.654
QUA	0.999**	−0.654	1

Table 8
Output of OLSE for Diagonistic check.

Parameters	Coef	Eigenvalue	Condition Index
Intercept	−2.988	2.850	1.000
Concentration	1.507	0.149	4.377
Equilibrium time	0.007	0.001	66.631
R^2	0.999	F-test	1482.783 (0.001)
Kolmogorov_Smirnov	0.191 (0.200)	Shapiro-Wilk	0.958 (0.794)

regularization techniques, we aimed to enhance the robustness, interpretability, and predictive accuracy of our model estimation, ensuring a more reliable and efficient model validation process. Thus, we split the dataset into training and testing sets, and the training set was adapted to fit the regression models using the following estimators: Ordinary Least Squares (OLS), ridge regression, lasso regression, and elastic-net regression. Subsequently, we evaluated the model performance using the testing set. To enhance the robustness of our model evaluation, we applied k-fold cross-validation to the training set, with k set to 3. This technique involves splitting the training set into k subsets, training the model on k-1 subsets, and validating it on the remaining subset, repeating this process k times with different validation subsets each time. For each penalty parameter in the models (e.g., alpha for lasso and elastic-net), we calculated the average prediction error across the k folds using the mean squared error (MSE) metric. The results are available in Table 9. Notably, lasso regression yielded the most favorable outcome, as evidenced by its minimum mean squared error prediction compared to the other models. The elastic-net and Ridge estimator competes favorably. Therefore, based on the Lasso estimate, concentration and equilibrium has a positive contribution on the quantity adsorbed.

We investigated the effect of time on the quantity adsorbed, considering different concentrations, which we analyzed in Table 10. In Table 10, the model intercept represents the estimated constant term in the regression equation, which signifies the predicted value of the response variable when all predictor variables are zero. The 'time' variable refers to the time duration for the adsorption to take place. The 't' column in the table represents the t-statistic, which measures the significance of each predictor variable's coefficient in the regression model. The 'sig' column indicates the statistical significance level (often denoted as the p-value) associated with each predictor variable's coefficient. A sig. value less than a 5 % level of significance suggests that time is statistically significant in explaining the variability of the quantity adsorbed. The result in Table 10 revealed that time had a positive impact on the concentrations. The positive impacts therefore account for the economical friendliness of the system in study. However, we further examined the relationship between different concentrations using an analysis of variance in Table 11. The results specified that there was no significant relationship among the varying concentrations since the p-value (0.591) exceeded the threshold of 0.05.

Table 9

Validation output.

Coef.	OLSE	Ridge	Lasso	Elastic-net
Intercept	−2.99	−12.2	−1.53	−3.24
Concentration	1.51	1.30	1.49	1.48
Equilibrium time	0.007	0.028	0.005	0.008
MSE	0.3710	0.0581	0.0415	0.0423

Table 10

Output for Regression on Quad. on time.

Concentration	Model	Unstandardized Coefficients		t	sig
		B	Std. Error		
2.5 mg/L	Intercept	−0.612	2.601	−2.35	0.822
	Time	16.195	2.484	6.519	0.001
5 mg/L	Intercept	−2.635	2.423	−1.087	0.319
	Time	8.835	1.142	7.735	0.000
7.5 mg/L	Intercept	−2.515	2.199	−1.144	0.296
	Time	7.643	0.899	8.498	0.000
10 mg/L	Intercept	1.357	1.426	0.952	0.378
	Time	2.923	0.266	10.981	0.000

Table 11

Analysis of variance output.

	Sum of Squares	df	Mean Square	F	Sig.
Between Groups	60.500	30	2.017	0.931	0.591
Within Groups	19.500	9	2.167		
Total	80.000	39			

Table 12

Regression coefficients of temperature on RHPW.

Model	Unstandardized Coefficients		Standardized Coefficients		t	Sig.
	B	Std. Error	Beta			
(Constant)	104.848	5.374			19.510	0.033
temp	−0.535	0.150	−0.963		−3.578	0.174

We analyzed the effect of temperature on ICD adsorption onto RHPW. Table 12 presents our results, which indicated a negative relationship between temperature and ICD removal onto RHPW. Specifically, as temperature increased by one unit, RHPW removal efficiency decreased by approximately 0.535 units. This validates and quantifies the effects of temperature on RHPW-ICD system.

3.10. Comparison of efficiency of RHPW with other adsorbents

Table 13 shows the assessment on the efficiency of RHPW compared to previously reported activated carbons. The performance of RHPW appeared to be fascinating and effective in the uptake of ICD due the recorded higher surface area in comparison to other

Table 13

Comparison of adsorption capacities of diverse adsorbents for ICD uptake.

S/N	Adsorbent name	Adsorbent surface area m^2/g	Initial concentration range (mg/L)	Monolayer quantity adsorbed (mg/g)	Reference
1	Silk	–	23.32–69.95	15.06	[76]
2	Fly ash	–	2.8–23.8	1.48	[77]
3	*Moringa oleifera* seed wastes	4.60	40	6.02	[78]
4	Palm-wood cellulose	–	10–40	5.43	[79]
5	Calcium hydroxide	–	5–50	0.95	[80]
6	*Acacia nicotica* saw dust	737.76	50–200	31.02	[81]
7	Palm kernel shells	331.89	10–20	20.57	[1]
8.	*Terminalia catappa*	29.03	600	26.77	[82]
9.	*Raphia hookerie* epicarp	945.43	2.5–15	20.41	This study

investigated adsorbents.

3.11. Cost analysis for Raphia hookerie adsorbent preparation

The cost of adsorbent's preparation is influenced by numerous parameters, including precursor, activating agent, and appliance operation costs [81,82]. A basic cost analysis was used to determine the possibility of commercialising RHPW derived from an abundant agricultural waste source. Table S1 presents the preparatory cost analysis of 1 kg of BSAB against commercially available activated carbon. The production cost was significantly lower than the average market cost of CAC, indicating the feasibility of commercialising RHPW.

4. Conclusion

The effectiveness of an agrowaste-based adsorbent in the uptake of commonly used dye (ICD) has been reported. The adsorbent prepared via orthophosphoric acid activation of *Raphia hookeri* fruit epicarp was effective in the removal of Indigo carmine dye (ICD). The isoelectric point of RHPW obtained at pH of 5 and decreased adsorption after the pH of 5 suggests that electrostatic repulsion occurred on RHPW surface after pH 5. While a multilayer adsorption occurred within the RHPW-ICD system, chemisorption dominates as indicated by the D-R model and PSO kinetics. The adsorption capacity (monolayer) was found to be 20.41 mg/g. The thermodynamic studies revealed that the effect of temperature on RHPW-ICD adsorption system is exothermic in nature. The Lasso estimate validated the effects of concentration and equilibrium time on quantity adsorbed hence justifies the economy of the system studied. The findings of this study revealed that RHPW could be an effective substitute adsorbent material for future large-scale industrial wastewater treatment. The concept of this study investigated ICD as a food dye, hence the low concentration investigated. However, ICD has several other applications in textile, cosmetics, pharmaceuticals and plastic industries which could require its use in larger concentrations. Adsorption at higher concentration and multicomponent effluent treatment is therefore recommended for future considerations.

Data availability statement

Data included in study/supplementary material/referenced in study.

CRediT authorship contribution statement

Adejumoke A. Inyinbor: Writing – review & editing, Supervision, Project administration, Methodology, Formal analysis, Data curation, Conceptualization. **Deborah T. Bankole:** Writing – review & editing, Project administration, Methodology, Formal analysis, Data curation. **Pamela Solomon:** Writing – original draft, Investigation, Formal analysis, Data curation. **Temitope S. Ayeni:** Visualization, Formal analysis. **Adewale F. Lukman:** Writing – review & editing, Visualization, Validation, Software.

Declaration of competing interest

The authors declare that they have no known competing financial interests or personal relationships that could have appeared to influence the work reported in this paper.

Appendix A. Supplementary data

Supplementary data to this article can be found online at https://doi.org/10.1016/j.heliyon.2024.e32121.

References

[1] G. Agbor Tabi, et al., Non-linear modelling of the adsorption of Indigo Carmine dye from wastewater onto characterized activated carbon/volcanic ash composite, Arab. J. Chem. 15 (1) (2022) 103515, https://doi.org/10.1016/j.arabjc.2021.103515.
[2] L.L. Zhi, M.A.A. Zaini, Potassium carbonate-treated palm kernel shell adsorbent for Congo red removal from water, J. Teknol. 75 (1) (2015) 233–239.
[3] M.O. Aremu, A.O. Arinkoola, I.A. Olowonyo, K.K. Salam, Improved phenol sequestration from aqueous solution using silver nanoparticle modified Palm Kernel Shell Activated Carbon, Heliyon 6 (7) (2020), https://doi.org/10.1016/j.heliyon.2020.e04492.
[4] A. Kumar Biswal, M. Sahoo, P. Kumar Suna, L. Panda, C. Lenka, P. Kumari Misra, Exploring the adsorption efficiency of a novel cellulosic material for removal of food dye from water, J. Mol. Liq. 350 (2022), https://doi.org/10.1016/j.molliq.2022.118577.
[5] K.D. Alanazi, et al., Citric acid-cross linked with magnetic metal-organic framework composite sponge for superior adsorption of indigo carmine blue dye from aqueous solutions: characterization and adsorption optimization via Box–Behnken design, J. Mol. Struct. 1299 (2024), https://doi.org/10.1016/j.molstruc.2023.137131.
[8] M. Ismail, et al., Pollution, toxicity and carcinogenicity of organic dyes and their catalytic bio-remediation, Curr. Pharmaceut. Des. 25 (34) (2019) 3645–3663, https://doi.org/10.2174/1381612825666191021142026.
[9] M.E. Ristea, O. Zarnescu, Indigo carmine: between necessity and concern, J. Xenobiotics 13 (3) (2023) 509–528, https://doi.org/10.3390/jox13030033.
[10] S. Caprarescu, et al., Efficient removal of Indigo Carmine dye by a separation process, Water Sci. Technol. 74 (10) (2016) 2462–2473, https://doi.org/10.2166/wst.2016.388.

[11] M. Lécuyer, M. Deschamps, D. Guyomard, J. Gaubicher, P. Poizot, Electrochemical assessment of indigo carmine dye in lithium metal polymer technology, Molecules 26 (11) (2021), https://doi.org/10.3390/molecules26113079.

[12] E. Ortiz, V. Gómez-Chávez, C.M. Cortés-Romero, H. Solís, R. Ruiz-Ramos, S. Loera-Serna, Degradation of indigo carmine using advanced oxidation processes: synergy effects and toxicological study, J. Environ. Protect. 7 (12) (2016) 1693–1706, https://doi.org/10.4236/jep.2016.712137.

[13] A. Zaouak, A. Noomen, H. Jelassi, Gamma-radiation induced decolorization and degradation on aqueous solutions of Indigo Carmine dye, J. Radioanal. Nucl. Chem. 317 (1) (2018) 37–44, https://doi.org/10.1007/s10967-018-5835-z.

[14] S. Gopi, P. Balakrishnan, A. Pius, S. Thomas, Chitin nanowhisker (ChNW)-functionalized electrospun PVDF membrane for enhanced removal of Indigo carmine, Carbohydr. Polym. 165 (2017) 115–122, https://doi.org/10.1016/j.carbpol.2017.02.046.

[15] D. Temitope Bankole, A. Peter Oluyori, A. Abosede Inyinbor, Potent adsorbent prepared from Bilghia sapida waste material: surface chemistry and morphological characterization, Mater. Today Proc. 65 (8) (2022) 3665–3670, https://doi.org/10.1016/j.matpr.2022.06.238.

[16] O.S. Bello, M.A. Moshood, B.A. Ewetumo, I.C. Afolabi, Ibuprofen removal using coconut husk activated Biomass, Chem. Data Collect. 29 (2020) 100533, https://doi.org/10.1016/j.cdc.2020.100533.

[17] O.S. Bello, T.C. Alagbada, O.C. Alao, A.M. Olatunde, Sequestering a non-steroidal anti-inflammatory drug using modified orange peels, Appl. Water Sci. 10 (7) (2020), https://doi.org/10.1007/s13201-020-01254-8.

[18] A.A. Inyinbor, F.A. Adekola, G.A. Olatunji, Microwave-assisted urea modified crop residue in Cu2+ scavenging, Heliyon 6 (4) (2020) e03759, https://doi.org/10.1016/j.heliyon.2020.e03759.

[19] A.A. Inyinbor, D.T. Bankole, P. Solomon, Adsorptive removal of acetaminophen onto acid-modified Raphia hookeri fruit epicarp, Biomass Convers. Biorefinery (2023), https://doi.org/10.1007/s13399-023-03871-0.

[20] F. Rassaei, Adsorption kinetics and isotherm modeling of lead in calcareous soils: insights into thermodynamics, desorption, and soil properties, Commun. Soil Sci. Plant Anal. 54 (15) (2023) 2059–2076, https://doi.org/10.1080/00103624.2023.2211116.

[22] A. Dahiya, A. Bhardwaj, A. Rani, M. Arora, J.N. Babu, Reduced and oxidized rice straw biochar for hexavalent chromium adsorption: revisiting the mechanism of adsorption, Heliyon 9 (11) (2023), https://doi.org/10.1016/j.heliyon.2023.e21735.

[23] B.H. Cheng, R.J. Zeng, H. Jiang, Recent developments of post-modification of biochar for electrochemical energy storage, Bioresour. Technol. 246 (2017) 224–233, https://doi.org/10.1016/j.biortech.2017.07.060.

[24] F. Rassaei, Sugarcane bagasse biochar affects corn (Zea mays L.) growth in cadmium and lead-contaminated calcareous clay soil, Arabian J. Geosci. 16 (3) (2023), https://doi.org/10.1007/s12517-023-11425-3.

[25] Y.Y. Ye, T.T. Qian, H. Jiang, Co-loaded N-doped biochar as a high-performance oxygen reduction reaction electrocatalyst by combined pyrolysis of biomass, Ind. Eng. Chem. Res. 59 (35) (2020) 15614–15623, https://doi.org/10.1021/acs.iecr.0c03104.

[26] W.H. Chen, et al., Biomass-derived biochar: from production to application in removing heavy metal-contaminated water, Process Saf. Environ. Protect. 160 (2022) 704–733, https://doi.org/10.1016/j.psep.2022.02.061.

[27] D.C.C. da S. Medeiros, et al., Pristine and engineered biochar for the removal of contaminants co-existing in several types of industrial wastewaters: a critical review, Sci. Total Environ. 809 (2022), https://doi.org/10.1016/j.scitotenv.2021.151120.

[28] A.A. Inyinbor, F.A. Adekola, G.A. Olatunji, Copper scavenging efficiency of adsorbents prepared from Raphia hookeri fruit waste, Sustain. Chem. Pharm. 12 (December 2018) (2019) 100141, https://doi.org/10.1016/j.scp.2019.100141.

[29] A.A. Inyinbor, F.A. Adekola, G.A. Olatunji, Kinetics, isotherms and thermodynamic modeling of liquid phase adsorption of Rhodamine B dye onto Raphia hookerie fruit epicarp, Water Resour. Ind. 15 (2016) 14–27, https://doi.org/10.1016/j.wri.2016.06.001.

[30] C.Y. Abasi, A.A. Abia, J.C. Igwe, Adsorption of iron (III), lead (II) and cadmium (II) ions by unmodified Raphia palm (Raphia hookeri) fruit endocarp, Environ. Res. J. 5 (3) (2011) 104–113, https://doi.org/10.3923/erj.2011.104.113.

[31] D.T. Bankole, A.P. Oluyori, A.A. Inyinbor, Acid-activated Hibiscus sabdariffa seed pods biochar for the adsorption of Chloroquine phosphate: prediction of adsorption efficiency via machine learning approach, South Afr. J. Chem. Eng. 42 (September) (2022) 162–175, https://doi.org/10.1016/j.sajce.2022.08.012.

[32] D.T. Bankole, A.P. Oluyori, A.A. Inyinbor, The removal of pharmaceutical pollutants from aqueous solution by Agro-waste, Arab. J. Chem. 16 (5) (2023) 104699, https://doi.org/10.1016/j.arabjc.2023.104699.

[33] K. Wang, et al., Comparing the adsorption of methyl orange and malachite green on similar yet distinct polyamide microplastics: uncovering hydrogen bond interactions, Chemosphere 340 (August) (2023), https://doi.org/10.1016/j.chemosphere.2023.139806.

[34] D. Drljača, D. Dragić, A. Borković, T. Botić, R. Jandrić, Removal of bemacid red dye by adsorption on sawdust and carbonized sawdust, Mater. Prot. 64 (1) (2023) 65–77, https://doi.org/10.5937/zasmat2301065D.

[35] J. Wu, H. Annath, H. Chen, C. Mangwandi, Upcycling tea waste particles into magnetic adsorbent materials for removal of Cr(VI) from aqueous solutions, Particuology 80 (2023) 115–126, https://doi.org/10.1016/j.partic.2022.11.017.

[36] Y. Sukmono, W.J. Ngu, T. Hadibarata, M. Syafrudin, Modeling of adsorption of copper on activated leaf-based biomass using response surface methodology (RSM), Biointerface Res. Appl. Chem. 13 (5) (2023) 1–11, https://doi.org/10.33263/BRIAC135.490.

[38] C.C. Okoye, O.D. Onukwuli, C.F. Okey-Onyesolu, Utilization of salt activated Raphia hookeri seeds as biosorbent for Erythrosine B dye removal: kinetics and thermodynamics studies, J. King Saud Univ. Sci. 31 (4) (2019) 849–858, https://doi.org/10.1016/j.jksus.2017.11.004.

[39] P.F. Tarbuka, R.H. Gumus, Methylene blue and iron (II) adsorption onto Raphia hookeri seed: a comparative equilibrium isotherm study, Int. J. Chem. Process Eng. Res. 8 (1) (2021) 11–18, https://doi.org/10.18488/journal.65.2021.81.11.18.

[40] R. Terungwa Iwar, K. Ogedengbe, "To cite this article raphael Terungwa Iwar, Kola Ogedengbe, Promise Okwuchukwu. Column studies on the adsorption of cadmium (Cd) in aqueous solution on Raffia palm seed (Raphia hookeri) activated carbon,", Am. J. Environ. Eng. Sci. 5 (3) (2018) 38–45 [Online]. Available: http://www.openscienceonline.com/journal/ajees.

[41] S. Ghogomu, N. Muluh, D.L. Ajifack, A.A.B. Alongamo, D.T. Noufame, Adsorption of lead (II) from aqueous solution using activated carbon prepared from Raffia palm (Raphia hookeri) fruit epicarp, IOSR J. Appl. Chem. (IOSR-JAC 9 (7) (2016) 74–85, https://doi.org/10.9790/5736-0907017485.

[42] S.F.A. Shattar, N.A. Zakaria, K.Y. Foo, One step acid activation of bentonite derived adsorbent for the effective remediation of the new generation of industrial pesticides, Sci. Rep. 10 (1) (2020), https://doi.org/10.1038/s41598-020-76723-w.

[43] O.A. Ekpete, A.C. Marcus, V. Osi, Preparation and characterization of activated carbon obtained from plantain (Musa paradisiaca) fruit stem, J. Chem. 2017 (2017), https://doi.org/10.1155/2017/8635615.

[45] S. Lagergren, "On the theory of so-called adsorption of dissolved substances," K. Sven, Vetenskapsakademiens Handl. 24 (4) (1898) 1–39.

[46] Y.S. Ho, G. McKay, Sorption of dye from aqueous solution by peat, Chem. Eng. J. 70 (2) (1998) 115–124, https://doi.org/10.1016/S1385-8947(98)00076-X.

[47] A.K. Ávila-Martínez, J.H. Roque-Ruiz, J. Torres-Pérez, N.A. Medellín-Castillo, S.Y. Reyes-López, Allura Red dye sorption onto electrospun zirconia nanofibers, Environ. Technol. Innov. 18 (1) (Jan. 2020) 1–12, https://doi.org/10.1016/j.eti.2020.100760.

[48] H.M. Freundlich, Over theadsorption in solution, Z. Phys. Chem. 57 (1906) 385–470.

[49] I. Langmuir, The constitution and fundamental properties of solids and liquids, J. Franklin Inst. 183 (1) (1917) 102–105, https://doi.org/10.1016/S0016-0032(17)90938-X.

[50] J.U. Ani, A.E. Ochonogor, K.G. Akpomie, C.S. Olikagu, C.C. Igboanugo, Abstraction of arsenic(III) on activated carbon prepared from Dialium guineense seed shell: kinetics, isotherms and thermodynamic studies, SN Appl. Sci. 1 (10) (2019) 1–11, https://doi.org/10.1007/s42452-019-1335-1.

[51] M. Dubinin, L.V. Radushkevich, Equation of the characteristic curve of activated charcoal proceedings of the academy of sciences, Phys. Chem. Sect. USSR 55 (1947) 331–333.

[52] Z.M. Şenol, Effective biosorption of Allura red dye from aqueous solutions by the dried-lichen (Pseudoevernia furfuracea) biomass, Int. J. Environ. Anal. Chem. 102 (16) (2022) 4550–4564, https://doi.org/10.1080/03067319.2020.1785439.

[53] Ihsanullah, et al., Effect of acid modification on adsorption of hexavalent chromium (Cr(VI)) from aqueous solution by activated carbon and carbon nanotubes, Desalination Water Treat. 57 (16) (2016) 7232–7244, https://doi.org/10.1080/19443994.2015.1021847.

[54] M.S. Reza, et al., Preparation of activated carbon from biomass and its' applications in water and gas purification, a review, Arab J. Basic Appl. Sci. 27 (1) (2020) 208–238, https://doi.org/10.1080/25765299.2020.1766799.

[55] O.S. Bello, O.C. Alao, T.C. Alagbada, O.S. Agboola, O.T. Omotoba, O.R. Abikoye, A renewable, sustainable and low-cost adsorbent for ibuprofen removal, Water Sci. Technol. 83 (1) (2021) 111–122, https://doi.org/10.2166/wst.2020.551.

[56] J.B. Njewa, T.T. Biswick, E. Vunain, C.S. Lagat, S.O. Lugasi, Synthesis and characterization of activated carbon from agrowastes for the removal of acetic acid from an aqueous solution, Adsorpt. Sci. Technol. 2022 (2022) 1–13, https://doi.org/10.1155/2022/7701128.

[58] S.A. Patil, et al., Dynamic adsorption of toxic indigo carmine dye on bio-inspired synthesised Fe3O4 nanoparticles: kinetic and thermodynamic study, Int. J. Environ. Anal. Chem. 102 (5) (2022) 1205–1227, https://doi.org/10.1080/03067319.2020.1734197.

[59] I.-H.T. Kuete, D.R.T. Tchuifon, G.N. Ndifor-Angwafor, A.T. Kamdem, S.G. Anagho, Kinetic, isotherm and thermodynamic studies of the adsorption of thymol blue onto powdered activated carbons from *Garcinia cola nut* shells impregnated with H$_3$PO$_4$ and KOH: non-linear regressi, J. Encapsulation Adsorpt. Sci. 10 (1) (2020) 1–27, https://doi.org/10.4236/jeas.2020.101001.

[60] I.H. Tiotsop Kuete, R.D. Tchuifon Tchuifon, A. Bopda, C. Sadeu Ngakou, G.N.A. Nche, S. Gabche Anagho, Adsorption of indigo carmine onto chemically activated carbons derived from the Cameroonian agricultural waste Garcinia cola nut shells and desorption studies, J. Chem. 2022 (2022), https://doi.org/10.1155/2022/1236621.

[63] M.B. Ahmad, U. Soomro, M. Muqeet, Z. Ahmed, Adsorption of Indigo Carmine dye onto the surface-modified adsorbent prepared from municipal waste and simulation using deep neural network, J. Hazard Mater. 408 (2021) 124433, https://doi.org/10.1016/j.jhazmat.2020.124433.

[66] K. Durairaj, P. Senthilkumar, V. Priya, P. Velmurugan, A.J. Kumar, Novel synthesis of chrysanthemum indicum flower as an adsorbenfor the removal of direct Congo red from aqueous solution, Desalination Water Treat. 113 (2018) 270–280, https://doi.org/10.5004/dwt.2018.22292.

[67] A. ul Haq, J. Shah, M.R. Jan, S. ud Din, Kinetic, equilibrium and thermodynamic studies for the sorption of metribuzin from aqueous solution using banana peels, an agro-based biomass, Toxicol. Environ. Chem. 97 (2) (2015) 124–134, https://doi.org/10.1080/02772248.2015.1041528.

[68] S. Ben-Ali, I. Jaouali, S. Souissi-Najar, A. Ouederni, Characterization and adsorption capacity of raw pomegranate peel biosorbent for copper removal, J. Clean. Prod. 142 (2017) 3809–3821, https://doi.org/10.1016/j.jclepro.2016.10.081.

[69] G.K. Latinwo, A.O. Alade, S.E. Agarry, E.O. Dada, Process optimization and modeling the adsorption of polycyclic aromatic-Congo red dye onto delonix regia pod-derived activated carbon, Polycycl. Aromat. Comp. 41 (2) (2021) 400–418, https://doi.org/10.1080/10406638.2019.1591467.

[70] J.O. Ojediran, A.O. Dada, S.O. Aniyi, R.O. David, A.D. Adewumi, Mechanism and isotherm modeling of effective adsorption of malachite green as endocrine disruptive dye using Acid Functionalized Maize Cob (AFMC), Sci. Rep. 11 (1) (2021) 1–15, https://doi.org/10.1038/s41598-021-00993-1.

[71] A.A. Inyinbor, et al., Chemometrics validation of adsorption process economy: case study of acetaminophen removal onto quail eggshell adsorbents, Sci. Afr. 19 (2023), https://doi.org/10.1016/j.sciaf.2022.e01471.

[73] Z.A. Alothman, A.Y. Badjah, O.M. Alduhaish, K. Rathinam, S. Panglisch, I. Ali, Synthesis, characterization, kinetics and modeling studies of new generation pollutant ketoprofen removal in water using copper nanoparticles, J. Mol. Liq. 323 (2021), https://doi.org/10.1016/j.molliq.2020.115075.

[76] N. Jiwalak, S. Rattanaphani, J.B. Bremner, V. Rattanaphani, Equilibrium and kinetic modeling of the adsorption of indigo carmine onto silk, Fibers Polym. 11 (4) (2010) 572–579, https://doi.org/10.1007/s12221-010-0572-2.

[77] T.E.M. De Carvalho, D.A. Fungaro, C.P. Magdalena, P. Cunico, Adsorption of indigo carmine from aqueous solution using coal fly ash and zeolite from fly ash, J. Radioanal. Nucl. Chem. 289 (2) (2011) 617–626, https://doi.org/10.1007/s10967-011-1125-8.

[78] M. El-Kammah, E. Elkhatib, S. Gouveia, C. Cameselle, E. Aboukila, Enhanced removal of Indigo Carmine dye from textile effluent using green cost-efficient nanomaterial: adsorption, kinetics, thermodynamics and mechanisms, Sustain. Chem. Pharm. 29 (June) (2022) 100753, https://doi.org/10.1016/j.scp.2022.100753.

[79] P.B. Wagh, V.S. Shrivastava, Removal of indigo carmine dye by using palm wood cellulose activated carbon in aqueous solution : a kinetic and equilibrium study, Int. J. Latest Technol. Eng. Manag. Appl. Sci. 4 (7) (2015) 106–114.

[80] T.N. Ramesh, D.V. Kirana, A. Ashwini, T.R. Manasa, Calcium hydroxide as low cost adsorbent for the effective removal of indigo carmine dye in water, J. Saudi Chem. Soc. 21 (2) (2017) 165–171, https://doi.org/10.1016/j.jscs.2015.03.001.

[81] T.B. Gupta, D.H. Lataye, Adsorption of indigo carmine and methylene blue dye: taguchi's design of experiment to optimize removal efficiency, Sadhana - Acad. Proc. Eng. Sci. 43 (10) (2018) 1–13, https://doi.org/10.1007/s12046-018-0931-x.

[82] L. Hevira, Rahmayeni Zilfa, J.O. Ighalo, R. Zein, Biosorption of indigo carmine from aqueous solution by Terminalia Catappa shell, J. Environ. Chem. Eng. 8 (5) (2020) 104290, https://doi.org/10.1016/j.jece.2020.104290.

Further reading

[6] M.C.D. Ngaha, L.G. Djemmoe, E. Njanja, I.T. Kenfack, Biosorption isotherms and kinetics studies for the removal of 2,6-dichlorophenolindophenol using palm tree trunk (Elaeis guineensis), J. Encapsulation Adsorpt. Sci. 8 (3) (2018) 156–177, https://doi.org/10.4236/jeas.2018.83008.

[7] M.C.D. Ngaha, E. Njanja, G. Doungmo, A. Tamo Kamdem, I.K. Tonle, Indigo carmine and 2,6-dichlorophenolindophenol removal using cetyltrimethylammonium bromide-modified palm oil fiber: adsorption isotherms and mass transfer kinetics, Int. J. Biomater. 2019 (2019), https://doi.org/10.1155/2019/6862825.

[21] B.E. Tokula, A.O. Dada, A.A. Inyinbor, K.S. Obayomi, O.S. Bello, U. Pal, Agro-waste based adsorbents as sustainable materials for effective adsorption of Bisphenol A from the environment: a review, J. Clean. Prod. 388 (2023), https://doi.org/10.1016/j.jclepro.2022.135819.

[37] I.K. Kinoti, E.M. Karanja, E.W. Nthiga, C.M. M'Thiruaine, J.M. Marangu, Review of clay-based nanocomposites as adsorbents for the removal of heavy metals, J. Chem. 2022 (2022), https://doi.org/10.1155/2022/7504626.

[44] A.O. Dada, A.A. Inyinbor, O.S. Bello, B.E. Tokula, Novel plantain peel activated carbon–supported zinc oxide nanocomposites (PPAC-ZnO-NC) for adsorption of chloroquine synthetic pharmaceutical used for COVID-19 treatment, Biomass Convers. Biorefinery 13 (10) (2023) 9181–9193, https://doi.org/10.1007/s13399-021-01828-9.

[57] A.O. Dada, et al., Sustainable and low-cost Ocimum gratissimum for biosorption of indigo carmine dye: kinetics, isotherm, and thermodynamic studies, Int. J. Phytoremediation 0 (0) (2020) 1524–1537, https://doi.org/10.1080/15226514.2020.1785389.

[61] A.A. Inyinbor, et al., Surface functionalized plant residue in cu2+ scavenging: Chemometrics of operational parameters for process economy validation, South Afr. J. Chem. Eng. 40 (February) (2022) 144–153, https://doi.org/10.1016/j.sajce.2022.03.001.

[62] P.R. Rout, T.C. Zhang, P. Bhunia, R.Y. Surampalli, Treatment technologies for emerging contaminants in wastewater treatment plants: a review, Sci. Total Environ. 753 (2021), https://doi.org/10.1016/j.scitotenv.2020.141990.

[64] H.O. Chukwuemeka-Okorie, F.K. Ekuma, K.G. Akpomie, J.C. Nnaji, A.G. Okereafor, Adsorption of tartrazine and sunset yellow anionic dyes onto activated carbon derived from cassava sievate biomass, Appl. Water Sci. 11 (2) (2021) 1–8, https://doi.org/10.1007/s13201-021-01357-w.

[65] A. Mandal, N. Bar, S.K. Das, Phenol removal from wastewater using low-cost natural bioadsorbent neem (Azadirachta indica) leaves: adsorption study and MLR modeling, Sustain. Chem. Pharm. 17 (May) (2020) 100308, https://doi.org/10.1016/j.scp.2020.100308.

[72] J.B. Chai, et al., Adsorption of heavy metal from industrial wastewater onto low-cost Malaysian kaolin clay–based adsorbent, Environ. Sci. Pollut. Res. 27 (12) (2020) 13949–13962, https://doi.org/10.1007/s11356-020-07755-y.

[74] A.F. Lukman, M. Arashi, V. Prokaj, Robust biased estimators for Poisson regression model: simulation and applications, Concurrency Comput. Pract. Ex. 35 (7) (2023), https://doi.org/10.1002/cpe.7594.

[75] M.N. Akram, M. Amin, A.F. Lukman, S. Afzal, Principal component ridge type estimator for the inverse Gaussian regression model, J. Stat. Comput. Simulat. 92 (10) (2022) 2060–2089, https://doi.org/10.1080/00949655.2021.2020274.

[83] J. Ogunmodede, S.B. Akanji, O.S. Bello, Moringa oleifera seed pod-based adsorbent for the removal of paracetamol from aqueous solution: a novel approach toward diversification, Environ. Prog. Sustain. Energy 40 (4) (2021) 1–11, https://doi.org/10.1002/ep.13615.

[84] D. Ursueguía, E. Díaz, S. Ordóñez, Adsorbents selection for the enrichment of low-grade methane coal mine emissions by temperature and pressure swing adsorption technologies, J. Nat. Gas Sci. Eng. 105 (May) (2022), https://doi.org/10.1016/j.jngse.2022.104721.